arXiv:1403.4787v2 [cond-mat.mtrl-sci] 21 Mar 2014

Intrinsic Oxygen Vacancy and Extrinsic Aluminium Dopant Interplay: A Route to the Restoration of Defective TiO_2

Conn O'Rourke[*,†,‡,¶] and David R. Bowler[†,‡,¶]

London Centre for Nanotechnology, 17-19 Gordon St, London, WC1H 0AH, Department of Physics & Astronomy, University College London, Gower St, London, WC1E 6BT, and UCL Satellite, International Centre for Materials Nanoarchitectonics (MANA), National Institute for Materials Science (NIMS), 1-1 Namiki, Tsukuba, Ibaraki 305-0044, Japan

E-mail: ucapcor@ucl.ac.uk

[*]To whom correspondence should be addressed
[†]LCN
[‡]UCL
[¶]UCL Satellite, MANA

Abstract

Density functional theory (DFT) and DFT corrected for on-site Coulomb interactions (DFT+U) calculations are presented on Aluminium doping in bulk TiO_2 and the anatase (101) surface. Particular attention is paid to the mobility of oxygen vacancies throughout the doped TiO_2 lattice, as a means by which charge compensation of trivalent dopants can occur. The effect that Al doping of TiO_2 electrodes has in dye sensitised solar cells is explained as a result of this mobility and charge compensation. Substitutional defects in which one Al^{3+} replaces one Ti^{4+} are found to introduce valence band holes, while intrinsic oxygen vacancies are found to introduce states in the band-gap. Coupling two of these substitutional defects with an oxygen vacancy results in exothermic defect formation which maintain charge neutrality. Nudged elastic band calculations have been performed to investigate the formation of these clustered defects in the (101) surface by oxygen vacancy diffusion, with the resulting potential energy surface suggesting energetic gains with small diffusion barriers. Efficiency increases observed in dye sensitised solar cells as a result of aluminium doping of TiO_2 electrodes are investigated by adsorbing the tetrahydroquinoline C2-1 chromophore on the defective surfaces. Adsorption on the clustered extrinsic Al^{3+} and intrinsic oxygen vacancy defects are found to behave as if adsorbed on a clean surface, with vacancy states not present, while adsorption on the oxygen vacancy results in a down shift of the dye localised states within the band-gap and defect states being present below the conduction band edge. Aluminium doping therefore acts as a benign dopant for 'cleaning' TiO_2 through oxygen vacancy diffusion.

Introduction

Titanium dioxide (TiO_2) has a wide variety of technological uses to which the considerable scientific interest in its surface properties can be attributed. For example TiO_2 is used in photocatalysis[1,2] and in dye sensitised solar cells (DSSCs).[3] DSSCs have been receiving widespread attention recently as a possible a clean, cost-effective renewable energy source.

Crystal defects can have a significant role in defining the properties of TiO_2, and therefore the electrodes used in DSSCs. Actively doping TiO_2 with nitrogen, for example, is known to lower the photo-excitation threshold in anatase TiO_2,[4,5] an extrinsic defect which has been put to use in photo-catalysis.[2] Aluminium dopants can be introduced in TiO_2 by inclusion of aluminium butoxide during the hydrolysis of titanium iso-propoxide (TTIP)[6] to form TiO_2. DSSC electrodes including aluminium dopants produced in this manner have been shown to decrease the concentration of Ti^{3+} defects resulting from oxygen vacancies, improve the open circuit voltage (V_{OC}) and thereby the DSSC efficiency,[6] however the mechanism has not been fully understood. Intrinsic defects, such as oxygen vacancies, also have a important role in the chemical reactivity of TiO_2 surfaces. An example is dissociation of water at vacancy sites on rutile (110).[7]

Oxygen vacancies introduce localised band-gap states in TiO_2 resulting in the formation of Ti^{3+} ions[8,9] which can trap injected electrons, and act as recombination centres.[10] Oxygen plasma treatments of TiO_2 electrodes, which reduce the number of oxygen vacancies, have shown a marked increase in the short-circuit current of DSSCs,[11] which indeed suggests that vacancies have a negative effect on DSSC performance. An increase in recombination sites in a DSSC will lead to interception of injected electrons by either the redox couple in solution, or by back transfer to dyes. Similarly this increase in recombination can cause a down shift in the quasi-Fermi energy of electrons in the conduction band, and a subsequent reduction in the short circuit voltage V_{OC}.

Previous theoretical studies carried out on aluminium doped TiO_2 have examined the stability of bulk defects in both rutile and anatase. In the case of anatase, clustering of defects in which two Al dopants combined with oxygen vacancies was found to produce the most stable defect type.[12,13] However the migration of aluminium interstitials throughout the bulk anatase crystal was found impossible at industrial temperatures, due to large transition barriers.[12] Oxygen vacancies are known to preferentially occupy sub-surface sites in anatase (101),[14,15] with diffusion barriers that can be overcome at typical annealing temperatures.

Diffusion of these oxygen vacancies suggests another mechanism by which stable clustering of intrinsic and extrinsic defects may occur in aluminium doped TiO_2.

The object of this work is to examine the effect of aluminium doping on the majority anatase (101) surface,[16] and to understand the observed increase in DSSC efficiency which results. To this end density functional theory (DFT) calculations have been carried out to characterise the doped (101) surface, with a particular focus on the interplay between intrinsic oxygen vacancy defects and the extrinsic aluminium dopants. Defect stabilities have been calculated for aluminium defects with and without the presence of oxygen vacancies, in both the bulk and the (101) surface.

Nudged elastic band (NEB) calculations have also been performed to establish diffusion barriers for oxygen vacancies in the presence of aluminium dopants, and illustrate the possibility of the intrinsic extrinsic defect clustering. Finally the effect of these defects on the adsorption of a typical DSSC dye is examined.

Computational Detail

All calculations have been performed using the plane wave DFT code VASP.[17] Exchange and correlation effects were approximated by the generalised gradient approximation of Perdew and Wang[18] with core electron wavefunctions treated within the projector augmented wave method.[19] For both bulk and surface calculations a plane wave cut-off of 800 eV has been used, which we have tested and give total energies converged to within 0.06 eV of values at 700 eV for the bulk.

Calculated lattice parameters for the bulk anatase TiO_2 without defects can be seen in Fig. 1. Good agreement with experimental data and the results from the previous work can be seen, and we have used these bulk lattice parameters throughout the current investigation.

Periodic images of the defects will interact with one another, and in order to gauge the extent of this interaction in the bulk case we have taken one defect type (A2; see Fig. 2) and

Table 1: Calculated and experimental lattice parameters and bond lengths of bulk anatase TiO_2

	Expt.[20] (Å)	Ref (US PP's)[21] (Å)	This Work (Å)
Lattice Parameters			
a	3.782	3.817 (+0.9%)	3.804 (+ 0.6%)
c	9.502	9.710 (+2.2%)	9.698 (+ 2.1%)
Bond Lengths			
Equatorial	1.932	1.954 (+1.1%)	1.947 (+ 0.8%)
Apical	1.979	2.011 (+1.6%)	2.005 (+ 1.3%)

performed calculations for varying supercell dimensions. Supercells containing one defect with sizes of 2, 3, 4 and 5 unit cells have been examined. Supercell extension was along one minor lattice vector (a=3.817 Å) while the other two vectors were kept constant. A Monkhorst-Pack k-point mesh has been utilised throughout these calculations with dimensions of $6 \times 6 \times 3$ for the smallest supercell, varying to $3 \times 6 \times 3$ for the largest supercell and provided energies converged to within 1×10^{-5} eV. Relaxations were performed using the conjugate gradients method, and considered finished when forces on ions were less than 0.03 eV/Å.

For surface calculations a four layer triclinic unit cell containing 288 atoms, with cell dimensions illustrated in Fig. 1, was the clean starting point. In order to prevent spurious interactions between periodic slabs it was ensured that a vacuum layer of at least 10 Å separated images in the (101) direction for all calculations. A Monkhorst-pack grid of $2 \times 2 \times 1$ was utilised throughout surface calculations, and increased to $4 \times 4 \times 1$ for density of states calculations. Fixing the bottom layer to the relaxed bulk position, geometry relaxations were again performed with the conjugate gradient method until ionic forces were less than 0.03 eV/Å. Calculations on chromophore adsorption were performed following previous work,[21] and considered fully relaxed when forces on ions were less than 0.03 eV/Å. In the calculation of defect stability isolated molecule calculations have been performed, and in each case the cell dimensions are the same as the substrate to which they will be compared.

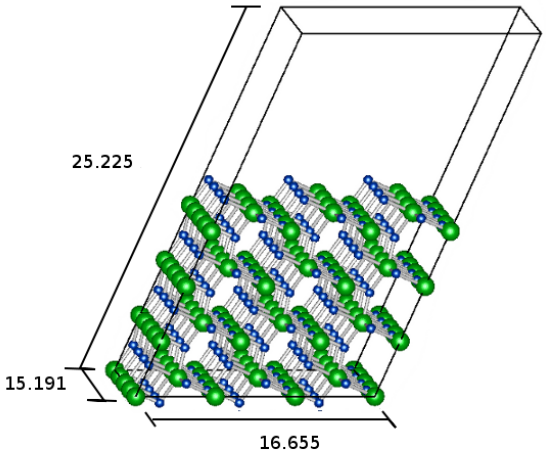

Figure 1: Anatase (101) surface: 4 layer slab used in defect calculations. Titanium atoms are represented in green, oxygen atoms in blue. The bounding box shows the unit cell with the cell dimensions in Å.

Results reported for the A2 and A3 defects have been obtained with spin unpolarised calculations. In the case of the A1 defect, the single substitution of an Al dopant leaves one unpaired electron so spin polarised calculations are performed throughout.

Semi-local functionals such as PW91 are known to incorrectly describe the Ti^{3+} states resulting from an oxygen vacancy in TiO_2, due largely to self-interaction errors and the band gap underestimation.[22] A similar failure has been reported in the case of single aluminium dopants for TiO_2 in the Rutile phase.[23] While employing hybrid functionals has been shown to more accurately describe these localised states in defective TiO_2, in plane wave codes such as VASP the use of hybrid functionals introduces an extra order of magnitude of computational time, which is a significant burden on the computational scientist.

We do not feel that the extra computational effort is justified here. As such as a step to rectify the limitations of GGA in the case of single Al substitutional defects and isolated oxygen vacancies, we have also performed GGA corrected for on-site Coulomb interactions (GGA+U),[24,25] employing the GGA+U correction in the form of Dudarev.[24] Hybrid functionals themselves are not fully characterised, as the fraction of exchange varies between

functionals (which makes them, at least in principle, as empirical as DFT+U) and we feel that GGA+U is the more pragmatic approach given the size of the systems under study.

While recent developments have suggested a route to the calculation of U self-consistently,[26] there is insufficient data on this approach to trust it absolutely. Therefore we must fit the value of U used to the problem under consideration, and this is one of the standard approaches to its use. As it is a relatively simple model, a single value of U will not fit different circumstances (and indeed a self-consistent U would give different values in different environments). Therefore in the case of the oxygen vacancy U with a value of 3eV has been applied to the Ti 3d orbitals, which has been shown to qualitatively agree with the B3LYP hybrid functional in the case of oxygen vacancies in Anatase TiO_2.[27] A range of values of U are applied to the O 2p states in the case of a single Al^{3+} for Ti^{4+} substitution in the bulk, with a value of 6eV used for surface calculations.

Bulk Defects

Previous studies have suggested that interstitial defects are relatively less stable than substitutional doping,[12] so here we focus only on these substitutional defect types. This is consistent with experimental evidence for the aluminium doping of rutile suggesting that Al will substitutionally replace Ti atoms.[28,29] Four different defects are considered in the bulk (illustrated in Fig. 2); direct substitution of a titanium atom with an aluminium atom (A1), two substitutional defects combined with an oxygen vacancy (A2 & A3) and a single substitutional defect combined with an oxygen vacancy (A4).

Alminium dopants may also be introduced in TiO_2 during the growth from the combustion of $TiCl_4$ by inclusion of $AlCl_3$. As in the work of Shirley et al,[12] we use as a measure of defect stability the energy of reaction for the following equivalent reaction:

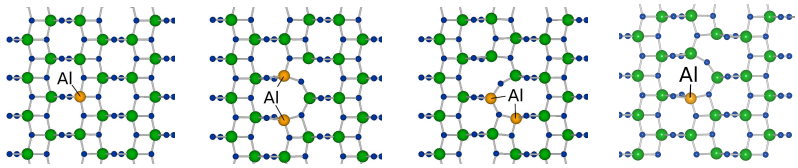

Figure 2: Aluminium doped anatase defect structues. Titanium atoms are represented in green, oxygen in blue, aluminium in orange. For clarity the defects are shown in a single (101) layer.

$$(x+z)\,\mathrm{TiO_2} + z\mathrm{AlCl_3} + \frac{z}{2}\mathrm{Cl_2} \rightleftharpoons \\ \mathrm{Ti}_x\mathrm{O}_y\mathrm{Al}_z + z\mathrm{TiCl_4} + \left(x+z-\frac{y}{2}\right)\mathrm{O_2} \tag{1}$$

such that

$$\begin{aligned}\Delta \mathrm{E}_{0K} =& \mathrm{E}_b\left(\mathrm{Ti}_x\mathrm{O}_y\mathrm{Al}_z\right) + \mathrm{E}_b\left(z\mathrm{TiCl_4}\right) \\ &+ \mathrm{E}_b\left(\left(x+z-\frac{y}{2}\right)\mathrm{O_2}\right) - \mathrm{E}_b\left(\frac{z}{2}\mathrm{Cl_2}\right) \\ &- \mathrm{E}_b((x+z)\,\mathrm{TiO_2}) - \mathrm{E}_b\left(z\mathrm{AlCl_3}\right)\end{aligned} \tag{2}$$

where $\Delta \mathrm{E}_{0K}$ is the energy of reaction at 0K, and $\mathrm{E_b}$ is binding energy as given by our DFT calculations. Zero point energies have been neglected.

As a first step we perform calculations on the A2 defect in order to evaluate the typical defect-defect interaction. Calculated bulk energies of reaction for the A2 defects in varying supercell sizes are exhibited in Table 2. Reaction energies suggest that defect-defect interaction is fairly short ranged, with energies at a defect separation along the varying vector of around 7Å converged to within 0.06 eV of that at a distance of around 11Å. In order to minimize the defect-defect interaction bulk calculations proceed with supercells of dimenisons

Table 2: Calculated ΔE_{0K} for bulk aluminium defect typei A2 with varying supercell size. Dimensions are given as multiples of unit cell vectors along the two minor and one major axis respectively.

Defect Type 85	A2 (eV)	
Supercell Dimension		Defect Separation (Å)
$2 \times 2 \times 1$	-0.051	3.81
$3 \times 2 \times 1$	-0.280	7.62
$4 \times 2 \times 1$	-0.342	11.44
$5 \times 2 \times 1$	-0.368	14.77

$4 \times 2 \times 1$ unit cells, containing 96 atoms in the clean supercell, giving a defect separation of greater than 7.5Å in all directions. Experimentally the atomic decomposition of the doped powder made up of 3.3% aluminium,[6] while cell dimensions $4 \times 2 \times 1$ give us 2.1% for A2 & A3 defects.

The calculated defect stability for each of the four defects examined can be seen in Table 3, and in the following subsections we discuss each of these bulk defects in turn.

A1 defect

Substitution of an Al^{3+} ion for a Ti^{4+} ion will result in one less electron in the system, and an oxygen hole being formed. Polaronic in nature, this resulting O^- state is poorly described by GGA and we have examined the defect stability and hole characteristics with varying values of on-site Coulomb interaction (U) Fig. 3.

Defect formation energy and O^- hole position can be seen to have a significant dependence on the value of the applied U correction (no value is reported for U=1 eV as convergence was not reached). Reaction energies vary over a wide range of around 1 eV. Similar ranges for reactions involving TiO_2 on varying U have been reported elsewhere.[30] In the case of pure GGA the hole is found to be delocalised throughout the system, and becomes increasingly more localised on an oxygen atom neighbouring the aluminium dopant as the value of U

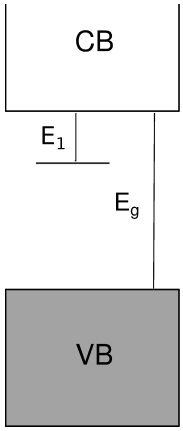

U(eV)	E_1	E_g (eV)	ΔE_{0K}
0	0.00	2.17	0.293
1	N/A	N/A	N/A
2	1.78	2.17	0.232
3	1.50	2.19	0.093
4	1.21	2.21	-0.076
5	0.92	2.23	-0.266
6	0.64	2.25	-0.472
7	0.39	2.26	-0.689

Figure 3: **A1 Bulk Defect:** U dependence on band gap (E_g), oxygen hole state (E_1) and defect formation energy (ΔE_{0K}).

is increased. Hartree-Fock studies of Al doped rutile TiO_2 find a well localised polaron associated with the dopant. Here we find that a U value of 6eV provides a well localised hole, which can be seen in Fig. 4, and is close to the value of 7eV used to describe the polaronic hole in rutile[23] and oxygen polarons in other materials.[31]

Selected bond lengths in the vicinity of the aluminium dopant can be seen in the case of pure GGA and GGA+U (U=6eV). In the case of the pure GGA calculation, variations in the bond lengths surrounding the dopant are found to be symmetric. Application of the onsite Coloumb correcton results in an asymmetric defect. Bond lengths involving an equatorially bonded oxygen atom adjacent to the dopant are extended, with this extension indicative of the associated O^- polaron (coordinates for this structure are provided as supporting information).

Energetically, as this hole becomes more localised with increased values of U, its position is shifted further from the valence band in the band gap. Partial density of states for the pure GGA defect and the GGA+U (U= 6eV) can be seen in Fig. 4(c). For uncorrected GGA the defect is unpolarised with the oxygen hole located at the top of the valence band, consistent with results reported by Shirley et al.[12] For the GGA+U solution the defect is polarised, with the localised hole in the band gap.

Table 3: Calculated ΔE_{0K} for bulk aluminium defect types with and without applied U correction.

Defect Type	GGA (eV)	GGA+U (U = 6eV)
A1	0.293	-0.472
A2	-0.388	-0.710
A3	-0.317	-0.629
A4	+2.143	N/A

A2 & A3 Defects

Calculated bulk energies of reaction for the A2 and A3 defects, and the comparative result for the A1 defect, are exhibited in Table 3. Given the wide variation of calculated reaction energies for the A1 defect formation with the value of the applied onsite Coloumb correction, we have also calculated the reaction energies for the A2 and A3 defects with an applied correction in order to make a direct comparison of the stability.

GGA predicts defect types comprising two aluminium substitutions with an oxygen vacancy, types A2 & A3, to be exothermic with the most stable defect type being A2. Single substitutional defect A1 is found to be endothermic by GGA. These results are in good agreement with previous work using the PBE functional, with ultrasoft pseudopotentials.[12] Substitution of an Al^{3+} for one Ti^{4+} results in one less electron in the system, and a O^{-} state is formed rather than O^{2-}. Combining two of these substitutions with an oxygen vacancy results in formal charge being maintained, giving the stability of defect types A2 & A3. While we can put less faith in the absolute values of the GGA+U results, given the empirical nature of the method and the lack of experimental data, the same trend is still exhibited with the clustered A2 and A3 defect types being more stable than a single Al^{3+} for Ti^{4+} substitution and a similar energy difference between A2 and A3 defects is found for both GGA and GGA+U.

A4 Defect

As a final defect type we have also examined the partial charge compensation of a single dopant combined with an oxygen vacancy. Defect stability for this A4 defect can also be seen in table 3, and we see that it is considerably less stable than the other three defects.

Calculations performed using GGA are reported as incorrectly delocalising oxygen vacancy states throughout the lattice with occupied states at the bottom of the conduction band.[22] As such we also apply the GGA+U method with a value of U=3eV to these states, which has been shown to correctly describe these Ti^{3+} defects qualitatively.[22] In bulk TiO_2 an oxygen vacancy results in the formation of occupied Ti^{3+} defect states in the gap.

The PDOS for both the pure GGA and the GGA+U solutions can be seen in Fig. 5 Both methods produce an occupied vacancy defect state at the bottom of the conduction band, which is delocalised throughout the lattice, while the oxygen hole associated with the Al dopant has been removed. This partial charge compensation can be seen as the most simple arrangement of an Al and vacancy defect leading to the clean up of Ti^{3+} states.

(101) Surface

In the case of the (101) surface numerous inequivalent positions are available for defects. The clean stoichiometric surface contains both five-fold and six-fold co-ordinated titanium atoms, each of which may be substituted for an Al atom. Energies of reaction for A2 and A3 defects in which substitutions occurred in different (101) layers were consistently found to be less stable than those containing two Al atoms in the same layer and therefore we only report the latter results. Differing defect positions for A2 defects can be seen in Fig. 6. For the A1 defect position the same notation applies, for example D1 corresponds to a single substitution of a five-fold co-ordinated Ti atom and D1.2 corresponds to substitution of a six-fold co-ordinated Ti in the upper layer. A3 defects necessarily contain Al substitutions at slightly differing positions along the [101] direction, which in the case of the uppermost

Table 4: Calculated ΔE_{0K} for differing positions in a 4 layer (101) slab. Most stable defect positions for each type are highlighted in bold. A1 GGA+U reaction energies are given relative to the bulk defect formation energy.

Defect Type	A1		A2	A3	A4
	GGA (eV)	GGA+U (eV)	GGA (eV)	GGA (eV)	GGA (eV)
Position					
D1	0.197	-0.056	-0.128	0.274	2.097
D1.2	0.454	0.333	0.625	0.331	2.514
D2	**-0.122**	**-0.225**	**-0.568**	**-0.337**	**1.663**
D2.2	0.043	0.094	-0.175	-0.299	1.931
D3	-0.050	0.164	-0.400	-0.299	1.800
D3.2	-0.020	0.328	-0.307	-0.301	1.854

layer means substitution of one five-fold co-ordinated and one six-fold co-ordinated Ti. The differing notation therefore refers to the position of the vacancy, with D1 refering to the defect in the uppermost layer with the vacancy slightly further along the [101] direction than D1.2.

Calculated reaction energies for defects at each of these positions are shown in table 4. It is known that oxygen vacancies on anatase (101) surfaces reside preferentially at sub-surface sites.[14,15] Sub-surface sites are here also found to be preferential for the aluminium defects, with the D2 position being the most stable for each type (the same was found in tests with 5 layer slabs). Large differences in stability can be seen between surface and subsurface sites, with energetic bias towards the sub-surface positions as much as 0.85 eV. Reaction energies tend to converge as the defect moves further into the bulk, and the highest energies are present when aluminium atoms reside next to two-fold cordinated oxygen atom, O(2), in the surface i.e. position D1.2. Despite residing next to an O(2) atom the A2 defect at position D1 is relatively more stable than its D1.2 counterpart as the Al atoms bonding to the O(2) atoms are themselves under co-ordinated as a result of being at the surface.

Given the empirical nature of the GGA+U reaction energies, the A1 GGA+U results are given relative to the bulk case in order to focus on the general trend rather than absolute

values. Similar energetic bias towards the subsurface D2 is exhibited, with the D1.2 position the least stable. GGA+U results for the A1 defect suggest that if the defect resides close enough to an under co-ordinated surface O(2) atom the O^- hole will localise on it. Defect positions D1, D1.2 and D2 all result with a surface localised hole state , as can be seen in Fig. 8. Indeed in the case of the D3.2 defect the hole localises on an O(2) atom in the bottom layer of the surface which, given that the bottom layer of the slab is fixed to the bulk position, explains the increase in the D3.2 defect formation energy relative to the bulk.

Energetically GGA predicts no variation in position relative to the valence band of the hole state, while for the GGA+U calculations a large energetic variation is observed with differing location in the surface Fig. 8. At the surface the hole state is found energetically further from the valence band, converging towards the bulk value as it moves away from the surface into the slab. This effect may be seen for two examples in Fig. 7 (D3.2 being the exception again, due to the localisation of the hole on a fixed atom).

As in the bulk case, the most stable defect is found to be that of type A2 and its formation is energetically favourable when at the D2 sub-surface position. Similarly, as in the bulk case, defect A4 is significantly less stable than the other three defect types. An important difference to note is that GGA predicts that when A1 defects reside at subsurface sites the defect formation becomes exothermic and energetically favourable, unlike the bulk which is endothermic. It is worth noting that the differences between all three defect stabilities are not so large, with ~ 0.2 eV differences between the calculated stabilities for the A1 and A3 defects, and the A3 and A2 defects respectively.

Oxygen Vacancy

We have seen that introduction of an Al dopant produces hole states in the band gap. Intrinsic oxygen vacancies have the opposite effect, introducing occupied states within the band gap. In the case of GGA these states are delocalised throughout the lattice, and unpolarised with the introduced states both at the bottom of the conduction band. Application

of DFT+U produces a localised vacancy state on a neighbouring Ti atom, giving us a Ti^{3+} ion, and a second delocalised throughout the lattice (spin difference isodensity plot may be seen in Fig. 9). We can see from the partial density of states that both states lie relatively close to the conduction band edge, with the localised state further into the band gap. This is similar to the situation reported for oxygen vacancies in bulk anatase treated with GGA+U,[22] however in the bulk two different solutions are found for the U=3eV case, one with a localised vacancy state and a delocalised vacancy state and a second in which both states are localised. Here we find only one stable structure, which we assume is due to the surface perturbation of the structure relative to that of the bulk.

Vacancy Diffusion

Thus far we have examined several defects in which extrinsic dopants cluster with intrinsic oxygen vacancies without discussing how this clustering will occur. Previous work has suggested that the movement of aluminium interstitials throughout the anatase lattice is not energetically feasible.[12] Here we propose the diffusion of oxygen vacancies throughout the lattice as a mechanism by which Al dopants and oxygen vacancies can combine.

In order to investigate this possibility we have performed climbing image nudged elastic band (NEB) calculations,[32] using the GGA functional, to examine the energy profile along oxygen vacancy diffusion paths which would result in the formation of A2, A3 and A4 defects. For these calculations the computational expense has been eased by reducing the number of anatase layers in the slab to three (sub-surface defects in position D2, i.e. those in the second layer from the surface, remain the most energetically favoured in the three layer slab). Given the preference of oxygen vacancies to reside subsurface in anatase TiO_2 and their reported mobility,[33] we examine the diffusion of these subsurface oxygen vacancies towards the aluminium dopants, with diffusion proceeding parallel to the (101) surface. This is taken as a viable mechanism for the combination of vacancies with dopants, given their

preference to reside sub-surface, although it is also entirely possible that vacancies could diffuse directly from the surface towards Al dopants.

Firstly a single oxygen vacancy diffusing towards a single A1 defect to form the A4 defect is examined, with the vacancy pathway and energy profile illustrated in Fig. 10. A clear enegetic bias ($\sim$ 0.2 eV) towards the formation of the A4 defect is exhibited, with an extremely small barrier of around 0.08 eV, which will be easily overcome at room temperature.

Next we consider the formation of A2 and A3 defects, again through the diffusion of oxygen vacancies towards Al dopants. It is worth noting that we have performed short tests using the NEB approach on the likelihood of substitutional Al dopants being able to traverse the lattice mediated by vacancies, but found significant energy barriers suggesting that Al dopants are indeed immobile. However given an experimental atomic composition of 3.3% aluminium in the doped TiO_2 powders,[6] and assuming that Aluminium is doped substitionally, Al dopants will occupy $\sim$ 10% of all lattice sites available. Each Ti lattice site is "coordinated" to 8 other Ti lattice sites, by which we mean there are 8 other adjacent Ti lattice sites which, when occupied by aluminium atoms, will arise in the proper configuration for either an A2 or A3 defect to be formed. Therefore the probability of two Al dopants residing adjacent to one another on the lattice of Ti sites in this manner is very significant. For example in a bulk supercell containing 60 atoms, at the experimental composition of 3.3%, there will be around two dopants. Each Ti lattice position available to these dopants is coordinated in the manner discussed to over 40% of remaining Ti lattice sites.

Therefore we examine the energetic barrier for oxygen vacancy diffusion towards two Al atoms residing adjacent to one another in the TiO_2 lattice, in order to gauge the typical energetic barrier

Potential energy surfaces and vacancy diffusion pathways for the formation of A2 and A3 defects can be seen in Figs. 11 and 12. Small diffusion barriers of around 0.15 eV and 0.1 eV are found for the A2 and A3 defects respectively, which will be easily overcome at room temperature. Energetic gains on overcoming these barriers of around 0.25 eV and 0.13

eV for A2 and A3 defects illustrate a bias towards the formation of these defects. Oxygen vacancy diffusion therefore provides a mechanism by which the aluminium dopants combine with oxygen vacancies in their proximity. This result explains the experimentally observed reduction in Ti^{3+} defects on doping of TiO_2 with aluminium.[6]

Electronic Structure & Chromophore Adsorption

Adsorption of a chromophore to TiO_2 electrodes is one of the fundamental interactions in a dye sensitised solar cell. To understand the impact of aluminium doping on this interaction calculations on a composite system in which a chromophore is adsorbed onto both clean and defective surfaces have been performed. For this purpose we have chosen the C2-1 tetrahydroquinoline chromophore which has shown to successfully sensitise TiO_2 in DSSCs.[34] The C2-1 chromophore is known to preferentially bind to the clean anatase (101) surface via a dissociative bidentate bridging mechanism[21] and it is this adsorption mode that is used throughout. The C2-1 dye has been adsorbed on surfaces containing the stable A2 and A3 clustered defects in subsurface positions, and compared with the adsorption on a surface containing an oxygen vacancy for comparison. Adsorption energies are calculated by the subtraction of the energy of the defective slab and the isolated C2-1 chromophore from that of the total system and are shown in Table 5. Adsorption on the slab containing a subsurface oxygen vacancy increases the adsorption energy significantly with respect to the clean surface, whereas the adsorption on slabs containing the aluminium defects vary only slightly with respect to the clean surface. Experimentally it has been reported that aluminium doped TiO_2 binds chromophores more strongly to the surface, due to a preference for dye molecules to attach to stable Ti^{4+} atoms rather than Ti^{3+}.[6] Our result that the C2-1 adsorption energy increases on the preferential subsurface oxygen vacancy compared to the Al defects suggests that this result is due to observed morphology changes resulting from the doping, not as a result of a decrease in Ti^{3+} concentration.

Table 5: Calculated adsorption energies for the C2-1 chromophore on the anatase (101) surface.

Defect type	Adsorption energy (eV)
Clean[21]	-1.14
O_V	-1.55
A2	-1.20
A3	-1.12

As we have already seen that in the A1 substitutional defect an Al^{3+} ion replacing a Ti^{4+} ion results in a valence band hole, while an oxygen vacancy introduces occupied Ti^{3+} states into the band-gap. The combination of two substitutional aluminium atoms with an oxygen vacancy (A2 & A3) causes the formal charge to be maintained, with the two electrons from the oxygen vacancy filling the valence band holes resulting from Al^{3+} substitutions. Oxygen vacancy states are not present and the substitutional valence band holes disappear, with the result that the doped A2 and A3 anatase surfaces behave as if they were clean. We can see this result on examining the density of states for the C2-1 adsorbed on the A2 defect and on the clean surface, Fig. 14, with little difference between the electronic structure for C2-1 adsorbed on the clean surface and that of the C2-1 adsorbed on the A2 (a similar result is found for the A3 defect).

Adsorption above the oxygen vacancy results in electronic structure that retains the occupied defect state at the bottom of the conduction band. This can be seen in Fig. 14 where the HOMO (at the zero on the x-axis) resides in the conduction band for the O_v case, while it is dye localised for the A2 & A3 cases (it is worth noting here that the result in Fig. 14 for the oxygen vacancy was obtained including the effects of spin polarisation but, with little difference observed between spin up and spin down, we report only the spin up result).

Interestingly the oxygen vacancy also down shifts the dye localised HOMO relative to the conduction band, while the A2 defect very slightly shifts these dye localised gap states closer to the conduction band. We have also performed adsorption calculations on the oxygen

vacancy with GGA+U (again using the PAW approach) and found a similar result, as can be seen in Fig. 15, with the oxygen vacancy defect states being retained just below the conduction band and a down-shift of the dye HOMO level within the band gap (in this case application of the GGA+U method provides the spin polarised result). As well as providing the reported recombination Ti^{3+} centres this shifting of the HOMO level by the introduction of an oxygen vacancy could have consequences for DSSC efficiency, potentially compounding the effect of recombination by adding to the reduction in J_{SC} and V_{OC}.

Conclusions

Density functional theory calculations on the Al^{3+} doping of anatase TiO_2 have been performed, with both the bulk and (101) surface examined. Single substitutions of Al^{3+} with Ti^{4+} (defect A1) and clustering of two of these extrinsic Al^{3+} dopants with an intrinsic oxygen vacancy have been investigated (defect type A2 and A3). Defect types A1 were found to be endothermic in the bulk, and exothermic at sub-surface sites on the (101) surface. A2 and A3 were found to be exothermic in the bulk and also preferentially occupy sub-surface sites on the (101) surface.

Nudged elastic band calculations have illustrated that combination of an intrinsic vacancy and extrinsic Al^{3+} dopants to form stable defects is possible and likely through oxygen vacancy diffusion. Low energy barriers for this diffusion process with an energetic bias towards the formation of A2 and A3 defects have been found, and vacancy diffusion has been concluded to be a viable route to these clustered defects.

Susbstitution of Ti^{4+} with $A1^{3+}$ results in a valence band hole. Combining two of these substitutions with an O vacancy result in the formally neutral defects, A2 and A3, in which the typical oxygen vacancy Ti^{3+} states are not present and the valence band hole disappears. This 'cleaning up' of the oxygen vacancies in the TiO_2 subsurface by benign aluminium doping results in a reduction in Ti^{3+} states and explains the observed increase in DSSC

efficiency obtained as a result. Recombination at these Ti^{3+} sites effectively leads to a reduced J_{SC}, the open circuit voltage can also be reduced as a result of a down shift in the quasi-Fermi energy. Similary a reduction in J_{SC} could occur as a result of the observed vacancy induced downshift in dye localised states in the gap. Removing these defects can improve both J_{SC} and V_{OC}, and thereby improve efficiency.

Adsorption of a typical DSSC chromophore, the C2-1 tetraquinoline dye, on the defective surface has been investigated. Adsorption to the oxygen vacancy site is found to be the most energetically favoured, with the adsorption on the A2 and A3 defects behaving much like adsorption on a clean surface. The observed V_{OC} increase on aluminium doping of the TiO_2 electrodes in DSSCs is concluded to be as a result of the reduction in Ti^{3+} states, and not due to stronger binding.

Acknowledgements

C.O'R. is supported by the MANA-WPI project through a collaboration with Cambridge University, and D.R.B. was funded by the Royal Society. We thank Umberto Terranova and Rami Louca for useful discussions. This work made use of the facilities of HECToR, the UK's national high-performance computing service, which is provided by UoE HPCx Ltd at the University of Edinburgh, Cray Inc and NAG Ltd, and funded by the Office of Science and Technology through EPSRC's High End Computing Programme. Calculations were performed at HECToR through the UKCP Consortium which is funded by EPSRC grant EP/F040105. The authors acknowledge the use of the UCL Legion High Performance Computing Facility, and associated support services, in the completion of this work.

Supporting Information

Relaxed GGA+U (U=6eV) coordinates for the A1 defect are included in .xyz format. This information is available free of charge via the Internet at http://pubs.acs.org

References

(1) Fujishima, A.; Zhang, X.; Tryk, D. A. *Surface Science Reports* **2008**, *63*, 515 – 582.

(2) Asahi, R.; Morikawa, T.; Ohwaki, T.; Aoki, K.; Taga, Y. *Science* **2001**, *293*, 269–271.

(3) O'Regan, B.; Grtzel, M. *Nature* **1991**, *353*, 737–740.

(4) Livraghi, S.; Paganini, M. C.; Giamello, E.; Selloni, A.; Di Valentin, C.; Pacchioni, G. *Journal of the American Chemical Society* **2006**, *128*, 15666–15671.

(5) Di Valentin, C.; Pacchioni, G.; Selloni, A.; Livraghi, S.; Giamello, E. *The Journal of Physical Chemistry B* **2005**, *109*, 11414–11419.

(6) Ko, K. H.; Lee, Y. C.; Jung, Y. J. *Journal of Colloid and Interface Science* **2005**, *283*, 482 – 487.

(7) Henderson, M. A. *Surface Science* **1998**, *400*, 203 – 219.

(8) Nakamura, I.; Negishi, N.; Kutsuna, S.; Ihara, T.; Sugihara, S.; Takeuchi, K. *Journal of Molecular Catalysis A: Chemical* **2000**, *161*, 205 – 212.

(9) Lin, Z.; Orlov, A.; Lambert, R. M.; Payne, M. C. *The Journal of Physical Chemistry B* **2005**, *109*, 20948–20952.

(10) Weidmann, J.; Dittrich, T.; Konstantinova, E.; Lauermann, I.; Uhlendorf, I.; Koch, F. *Solar Energy Materials and Solar Cells* **1998**, *56*, 153 – 165.

(11) Kim, Y.; Yoo, B. J.; Vittal, R.; Lee, Y.; Park, N.-G.; Kim, K.-J. *Journal of Power Sources* **2008**, *175*, 914 – 919.

(12) Shirley, R.; Kraft, M.; Inderwildi, O. R. *Phys. Rev. B* **2010**, *81*, 075111.

(13) Steveson, M.; Bredow, T.; Gerson, A. R. *Phys. Chem. Chem. Phys.* **2002**, *4*, 358–365.

(14) Cheng, H.; Selloni, A. *Phys. Rev. B* **2009**, *79*, 092101.

(15) He, Y.; Dulub, O.; Cheng, H.; Selloni, A.; Diebold, U. *Phys. Rev. Lett.* **2009**, *102*, 106105.

(16) Zhang, H.; F. Banfield, J. *J. Mater. Chem.* **1998**, *8*, 2073–2076.

(17) Kresse, G.; Furthmller, J. *Computational Materials Science* **1996**, *6*, 15 – 50.

(18) Perdew, J. P.; Chevary, J. A.; Vosko, S. H.; Jackson, K. A.; Pederson, M. R.; Singh, D. J.; Fiolhais, C. *Phys. Rev. B* **1992**, *46*, 6671–6687.

(19) Kresse, G.; Joubert, D. *Phys. Rev. B* **1999**, *59*, 1758–1775.

(20) Burdett, J. K.; Hughbanks, T.; Miller, G. J.; Richardson, J. W.; Smith, J. V. *Journal of the American Chemical Society* **1987**, *109*, 3639–3646.

(21) O'Rourke, C.; Bowler, D. R. *The Journal of Physical Chemistry C* **2010**, *114*, 20240–20248.

(22) Finazzi, E.; Valentin, C. D.; Pacchioni, G.; Selloni, A. *The Journal of Chemical Physics* **2008**, *129*, 154113.

(23) Iwaszuk, A.; Nolan, M. *Journal of Physics: Condensed Matter* **2011**, *23*, 334207.

(24) Dudarev, S. L.; Botton, G. A.; Savrasov, S. Y.; Humphreys, C. J.; Sutton, A. P. *Phys. Rev. B* **1998**, *57*, 1505–1509.

(25) Anisimov, V. I.; Aryasetiawan, F.; Lichtenstein, A. I. *Journal of Physics: Condensed Matter* **1997**, *9*, 767.

(26) Kulik, H. J.; Cococcioni, M.; Scherlis, D. A.; Marzari, N. *Phys. Rev. Lett.* **2006**, *97*, 103001.

(27) Finazzi, E.; Valentin, C. D.; Pacchioni, G.; Selloni, A. *The Journal of Chemical Physics* **2008**, *129*, 154113.

(28) Stebbins, J.; Farnan, I.; Klabunde, U. *Journal of the American Ceramic Society* **1989**, *72*, 2198–2200, cited By (since 1996)20.

(29) Gesenhues, U.; Rentschler, T. *Journal of Solid State Chemistry* **1999**, *143*, 210 – 218.

(30) Hu, Z.; Metiu, H. *The Journal of Physical Chemistry C* **2011**, *115*, 5841–5845.

(31) Yeriskin, I.; Nolan, M. *Journal of Physics: Condensed Matter* **2010**, *22*, 135004.

(32) Henkelman, G.; Uberuaga, B.; Jnsson, H. *Journal of Chemical Physics* **2000**, *113*, 9901–9904.

(33) Cheng, H.; Selloni, A. *The Journal of Chemical Physics* **2009**, *131*, –.

(34) Chen, R.; Yang, X.; Tian, H.; Wang, X.; Hagfeldt, A.; Sun, L. *Chemistry of Materials* **2007**, *19*, 4007–4015.

Graphical TOC Entry

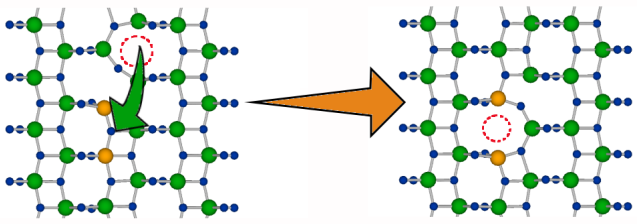

Diffusion of oxygen vacancy in the doped Anatase TiO_2 (101) sub-surface.

	Bond (Å)									
	Al-O1	Al-O2	Al-O3	Al-O4	Al-O5	Al-O7	O5-Ti2	O5-Ti3	O7-Ti4	O7-Ti5
Method										
GGA	1.91	1.90	1.93	1.93	1.91	1.91	2.04	1.88	2.02	1.89
GGA+U(6 eV.)	1.90	1.85	1.93	1.91	**1.95**	1.90	**2.29**	**2.07**	2.01	1.90

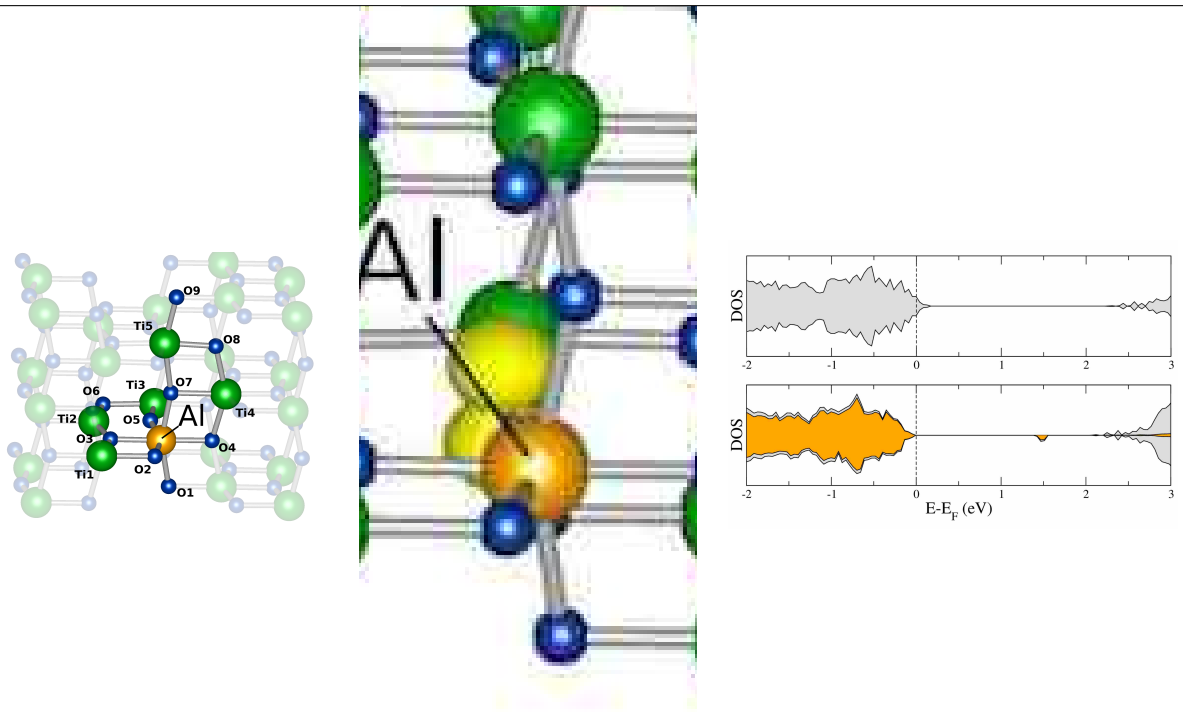

(a) **(b)** **(c)**

Figure 4: **A1 Bulk Defect: Top** Selected bond lengths for the A1 defect. Largest bond lengths resulting from a localised polaron are in bold. **Bottom (a)** Atom labels used in table above. **(b)** GGA+U(6eV) defect state with localised hole. Titaniumm atoms are represented in green, oxygen atoms in blue, aluminium in orange and spin difference isosurface in yellow. **(c)** Projected density of states for A1 defect. Top: GGA, Bottom: GGA+U (U=6eV). Total DOS in grey and for GGA+U calculations the oxygen 2p states are represented in orange.

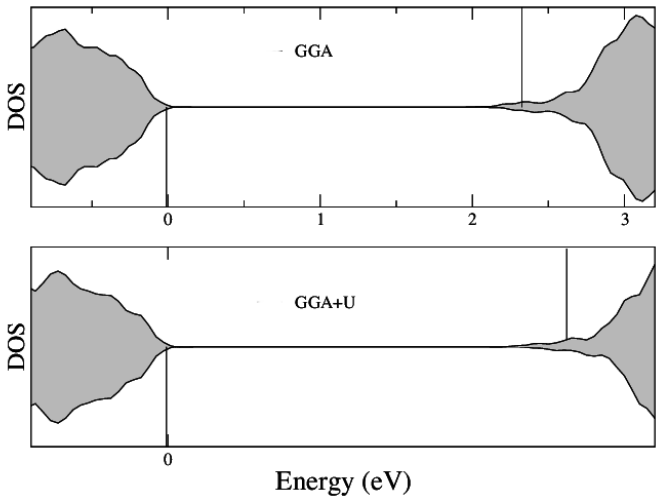

Figure 5: Partial density of states for A4 defect. The top of the valence band is at zero, with the highest occupied Kohn-Sham states for each spin channel illustrated with a vertical line.

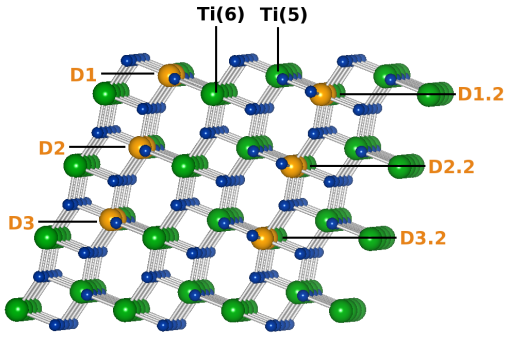

Figure 6: Notation for surface defect positions relative to the 101 surface. Titanium atoms are represented in green, oxygen atoms in blue and aluminium in orange. Ti(5) labels five-fold co-ordinated titanium atoms, Ti(6) six-fold coordinated.

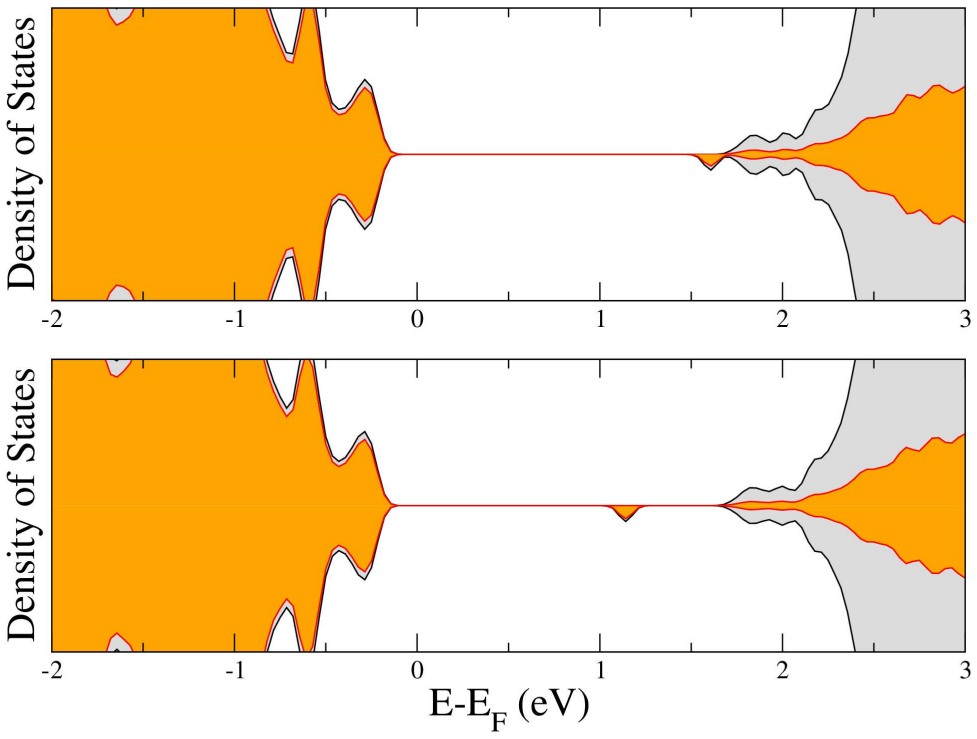

Figure 7: Partial density of states for single Al dopants in the (101) surface. Top: A1 defect in D1 surface position. Bottom: A1 defect in D2.2 position. Projection on the oxygen atoms is in orange, total DOS in grey.

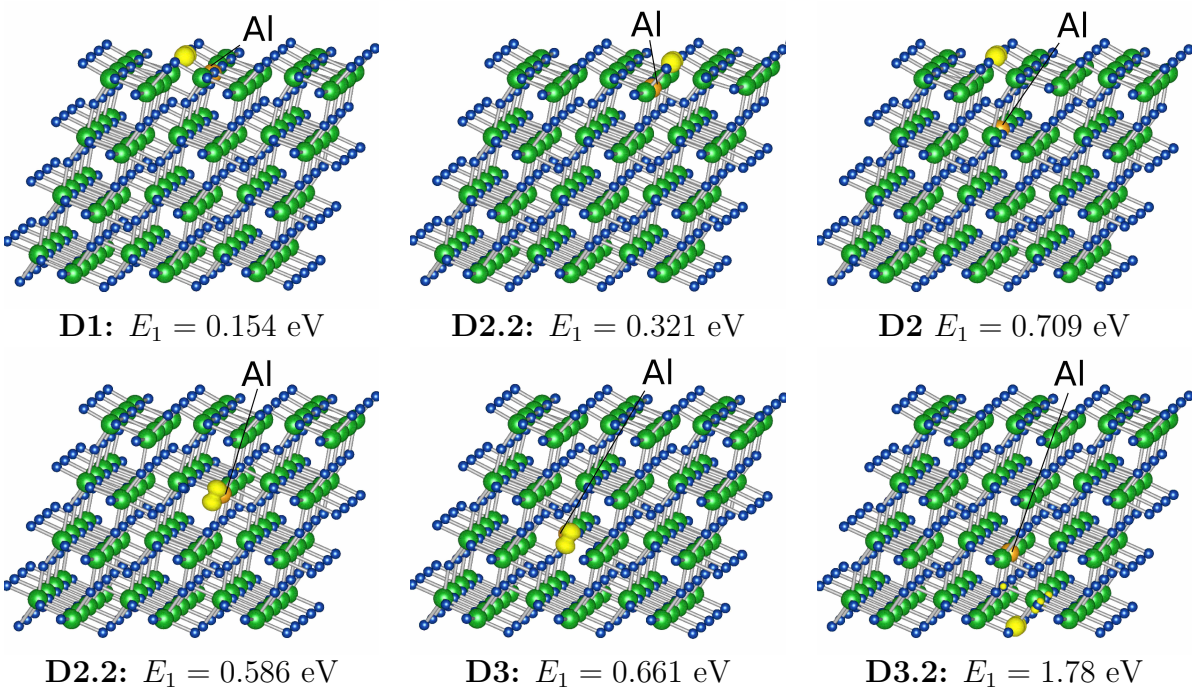

D1: $E_1 = 0.154$ eV **D2.2:** $E_1 = 0.321$ eV **D2** $E_1 = 0.709$ eV

D2.2: $E_1 = 0.586$ eV **D3:** $E_1 = 0.661$ eV **D3.2:** $E_1 = 1.78$ eV

Figure 8: **A1 Surface Defect:** GGA+U spin difference isosurface for the A1 single substitutional defect at varying positions in the (101) surface. Associated hole position relative to the conduction band is also given.

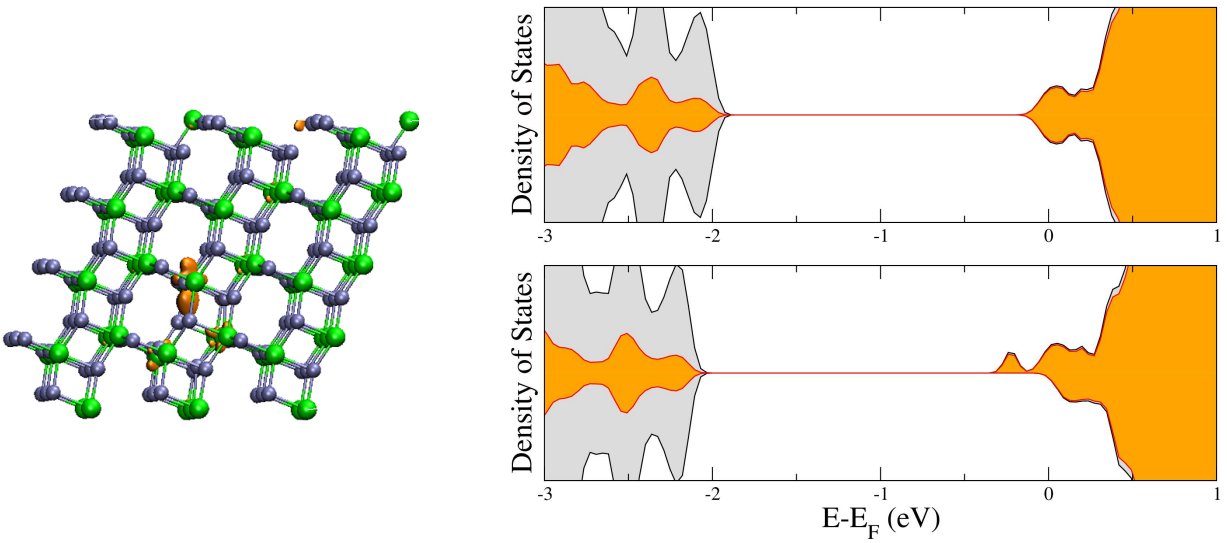

(a) **(b)**

Figure 9: **(a)** Spin isosurface for oxygen vacancy state in the (101) surface and **(b)**partial density of states for GGA(top) and GGA+U(U=3eV)(bottom)

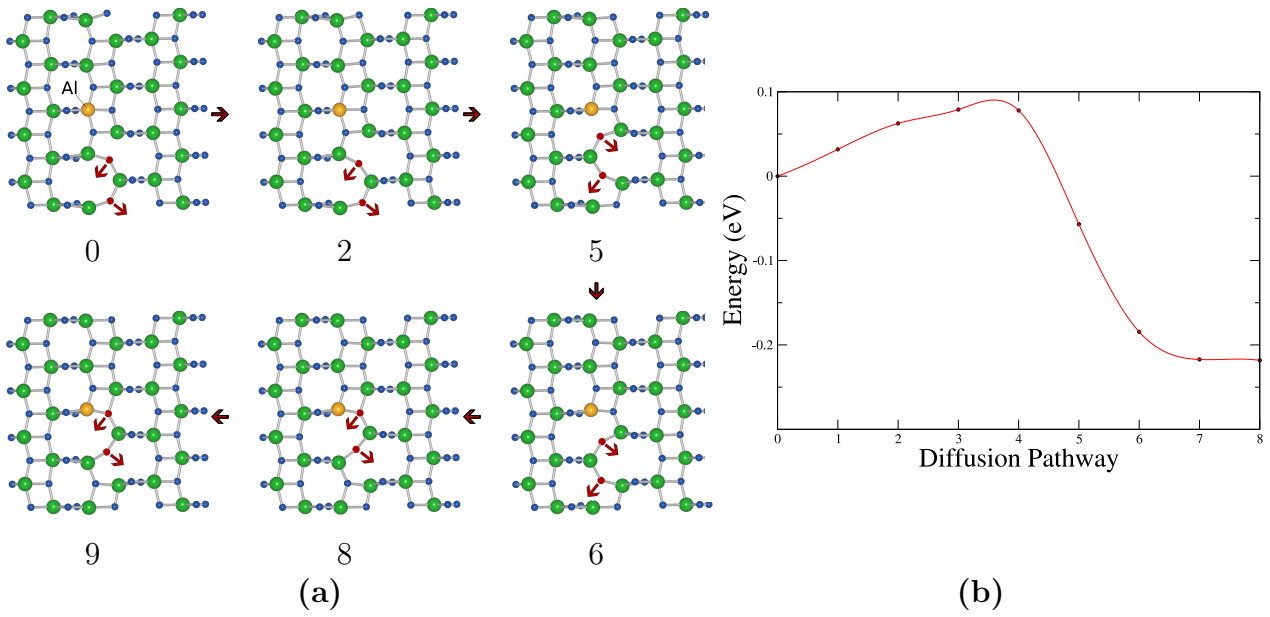

Figure 10: **(a)** Diffusion pathway for an oxygen vacancy towards Aluminium dopant resulting in a defect of A4 type. For clarity only the central layer is illustrated. **(b)** Potential energy pathway along the shown diffusion pathway, with a spline fitted to the data to serve as a guide to the eye.

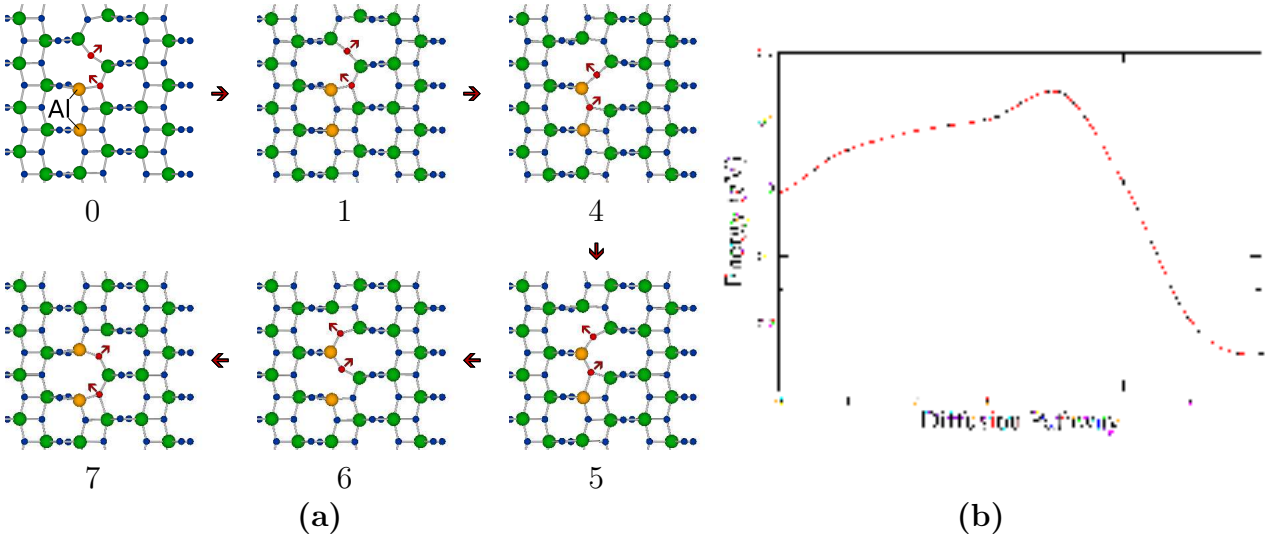

Figure 11: **(a)** Diffusion pathway for an oxygen vacancy towards Aluminium dopants resulting in a defect of A2 type. For clarity only the central layer is illustrated. **(b)** Potential energy pathway along the shown diffusion pathway, with a spline fitted to the data to serve as a guide to the eye.

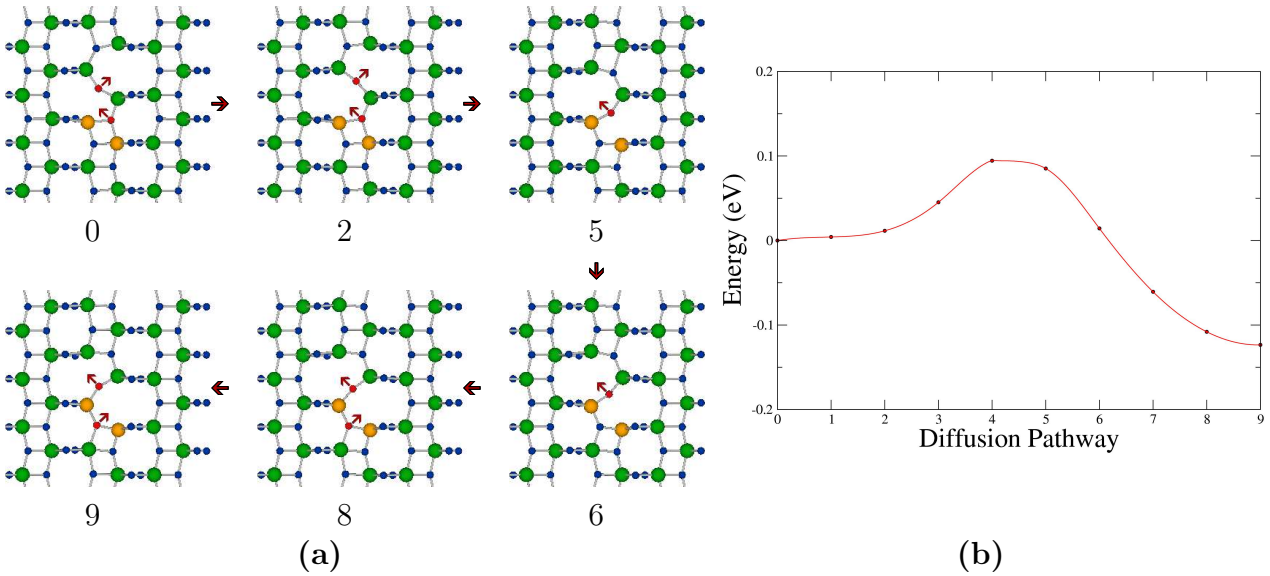

Figure 12: **(a)** Diffusion pathway for oxygen vacancy towards Aluminium dopants resulting in a defect of A3 type. For clarity only the central layer is illustrated. **(b)** Potential energy pathway along the shown diffusion pathway, with a spline fitted to the data to serve as a guide to the eye.

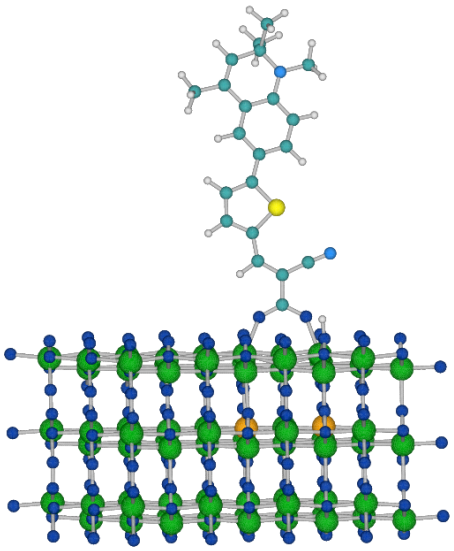

Figure 13: C2-1 chromophore adsorbed above a defect of A2 type in the anatase (101) surface.

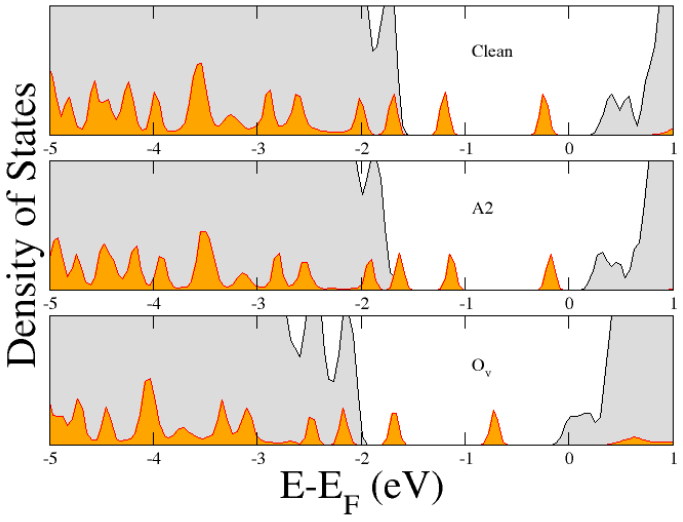

Figure 14: Partial density of states. Top: C2-1 adsorbed on clean anatase (101). Middle: C2-1 adsorbed on anatase (101) containing an A2 subsurface defect. Bottom: C2-1 adsorbed on anatase (101) containing an oxygen vacancy. The projection on the chromophore is in orange, total DOS in grey.

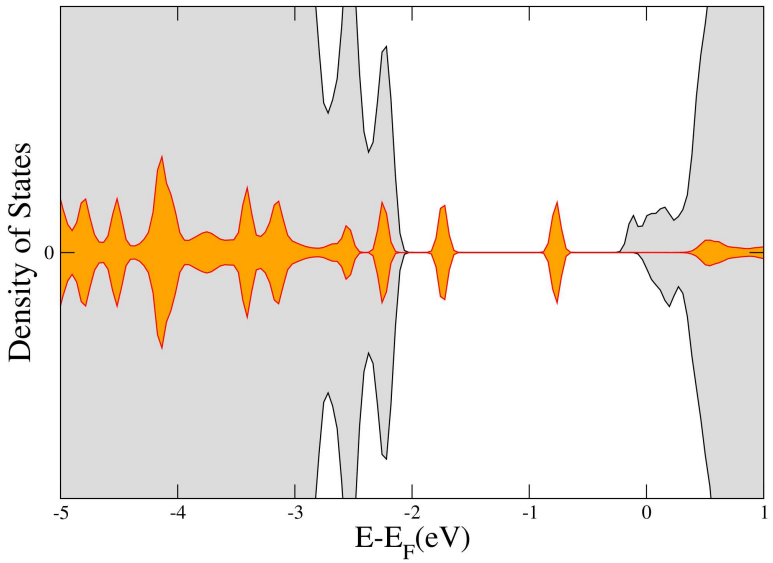

Figure 15: GGA+U partial density of states for C2-1 adsorbed above an oxygen vacancy. The projection on the chromophore is in orange, total DOS in grey.